British Journal of Pharmacology

DOI:10.1111/bph.13287
www.brjpharmacol.org

RESEARCH PAPER

Crucial role of the orexin-B C-terminus in the induction of OX_1 receptor-mediated apoptosis: analysis by alanine scanning, molecular modelling and site-directed mutagenesis

Pascal Nicole[1], Pierre Couvineau[1], Nadege Jamin[2], Thierry Voisin[1] and Alain Couvineau[1]

[1]*Faculté de Médecine Site Bichat, INSERM U1149/Inflammation Research Center (CRI), Paris-Diderot University, DHU UNITY, 16, rue H. Huchard, 75018 Paris, France, and* [2]*Laboratoire des Protéines et Systèmes Membranaires, CEA, iBiTecS, I2BC, F-91191 Gif-sur-Yvette Cedex, France*

Correspondence
Alain Couvineau, Faculté de Médecine Site Bichat, INSERM U1149/CRI, Paris-Diderot University, DHU UNITY, 16, rue H. Huchard, 75018 Paris, France.
E-mail: alain.couvineau@inserm.fr

Received
30 September 2014
Revised
12 June 2015
Accepted
11 August 2015

BACKGROUND AND PURPOSE

Orexins (A and B) are hypothalamic peptides that interact with OX_1 and OX_2 receptors and are involved in the sleep/wake cycle. We previously demonstrated that OX_1 receptors are highly expressed in colon cancer tumours and colonic cancer cell lines where orexins induce apoptosis and inhibit tumour growth in preclinical animal models. The present study explored the structure–function relationships of orexin-B and OX_1 receptors.

EXPERIMENTAL APPROACH

The contribution of all orexin-B residues in orexin-B-induced apoptosis was investigated by alanine scanning. To determine which OX_1 receptor domains are involved in orexin-B binding and apoptosis, a 3D model of OX_1 receptor docked to the orexin-B C-terminus (AA-20–28) was developed. Substitution of residues present in OX_1 receptor transmembrane (TM) domains by site-directed mutagenesis was performed.

KEY RESULTS

Alanine substitution of orexin-B residues, L^{11}, L^{15}, A^{22}, G^{24}, I^{25}, L^{26} and M^{28}, altered orexin-B's binding affinity. Substitution of these residues and of the Q^{16}, A^{17}, S^{18}, N^{20} and T^{27} residues inhibited apoptosis in CHO-S–OX_1 receptor cells. The K^{120}, P^{123}, Y^{124}, N^{318}, K^{321}, F^{340}, T^{341}, H^{344} and W^{345} residues localized in TM2, TM3, TM6 and TM7 of OX_1 receptors were shown to play a role in orexin-B recognition and orexin-B/OX_1 receptor-induced apoptosis.

CONCLUSIONS AND IMPLICATIONS

The C-terminus of orexin-B (i) plays an important role in its pro-apoptotic effect; and (ii) interacts with some residues localized in the OX_1 receptor TM. This study defines the structure–function relationship for orexin-B recognition by human OX_1 receptors and orexin-B/OX_1 receptor-induced apoptosis, an important step for the future development of new agonist molecules.

Abbreviations

CHARMM, chemistry at harvard macromolecular mechanics; CMAP, grid-based energy correction maps; ECL, extracellular loop; LINCS, Linear Constraint Solver; TM, transmembrane

Tables of Links

TARGETS	
GPCRs[a]	**Enzymes**[b]
OX_1 receptor	Caspase-3
OX_2 receptor	Caspase-7

LIGANDS	
IP_3	Orexin-B
Orexin-A	Suvorexant

These Tables list key protein targets and ligands in this article which are hyperlinked to corresponding entries in http://www.guidetopharmacology.org, the common portal for data from the IUPHAR/?BPS Guide to PHARMACOLOGY (Pawson *et al.*, 2014) and are permanently archived in the Concise Guide to PHARMACOLOGY 2013/?14 ([a,b]Alexander *et al.*, 2013a, b).

Introduction

Orexins A and B (also known as hypocretins 1 and 2) are hypothalamic 33-aminoacid and 28-aminoacid neuropeptides, respectively, which originate from prepro-orexin, a 131-residue precursor. Orexin-A contains two intramolecular disulfide bonds between positions 6 to 12 and 7 to 14, while orexin-B does not have any. These two peptides share the same effects, regulating sleep, wakefulness, feeding, energy homeostasis, obesity, diabetes, breathing, reward system or drug addiction (Laburthe and Voisin, 2012). Orexins trigger biological effects by interacting with two members of the class A GPCR family, that is, orexin receptor-1 (OX_1 receptor) and orexin receptor-2 (OX_2 receptor) (Thompson *et al.*, 2014). Activation of these receptors by orexins classically induces cellular calcium transients through Gq-dependent and Gq-independent pathways (Laburthe *et al.*, 2010). Besides these central actions, the orexins/receptor system is also involved in peripheral effects, including modulation of the cardiovascular system and the regulation of neuroendocrines and reproduction (Xu *et al.*, 2013). Recently, our group demonstrated that orexin-A and orexin-B, bound to OX_1 receptors, can induce massive apoptosis, resulting in the drastic reduction of cell growth in various colonic cancer cell lines, including HT-29, LoVo, Caco-2 and others (Voisin *et al.*, 2011). An entirely novel mechanism, not related to Gq-mediated phospholipase C activation, was shown to trigger orexin-induced apoptosis (Voisin *et al.*, 2008; El Firar *et al.*, 2009). In fact, orexins induced the tyrosine phosphorylation of two immunoreceptor tyrosine-based motifs (ITIMs) located at the interface between transmembrane (TM) domain 2 and TM 7 of the OX_1 receptor and the cytoplasm (Voisin *et al.*, 2008). The resulting phosphorylated receptor could then recruit and activate the phosphotyrosine phosphatase, SHP-2, which is responsible for mitochondrial apoptosis, involving cytochrome c release from mitochondria to cytosol and caspase-3 and caspase-7 activation (El Firar *et al.*, 2009). The pro-apoptotic effect of orexins has also been extended to other cancer cell lines derived from human neuroblastoma (SK-N-MC cell line) and rat pancreatic cancer (AR42J cell line) (Rouet-Benzineb *et al.*, 2004; Voisin *et al.*, 2006). Recent data demonstrated that the OX_1 receptors is aberrantly expressed in all resected primary colorectal tumours and liver metastases tested but is not present in normal colon tissues (Voisin *et al.*, 2011). Moreover, an injection of exogenous orexins to mice strongly reduced *in vivo* tumour growth and reversed the development of established tumours in mice xenografted with colon cancer cell lines such as HT-29 or LoVo, due to robust apoptosis induction (Voisin *et al.*, 2011). Taken together, these observations suggest that the orexins/ OX_1 receptor system may represent a new promising target in colorectal cancer therapy, and most probably in other cancers, including pancreatic cancers neuroblastoma, and/or prostate cancer (Alexandre *et al.*, 2014). In this context, structure–function relationship studies of the orexins/ OX_1 receptor system are essential for the development of new agonists of OX_1 receptors that may represent new therapeutic approaches.

Until now, little has been known about the structure–function relationship of the orexins/ OX_1 receptors system. The determination of the 3D structure of orexin-B in solution by 2D NMR spectroscopy revealed the presence of two α-helices encompassing residues Leu^7 to Gly^{19} and residues Ala^{23} to Met^{28}, connected by a short flexible loop (Lee *et al.*, 1999). In addition, pharmacological tools have been developed to discriminate between OX_1 and OX_2 receptors (Gotter *et al.*, 2012; Laburthe and Voisin, 2012), including selective peptide agonists for the OX_2 receptor such as [Ala^{11}, D-Leu^{15}] orexin-B6–28 (Asahi *et al.*, 2003), [Ala^{27}] orexin-B6–28 (Lang *et al.*, 2004), [Pro^{11}] orexin-B6–28 (Lang *et al.*, 2004) and other selective non-peptide antagonists, including TCS-orexin 2-29, JNJ-10397049, EMP4 for OX_2 receptors or the non-peptide molecule antagonists SB-334867, SB-408124 and SB-674042 for OX_1 receptors (review by Gotter *et al.*, 2012). Nevertheless, the residues of orexin-B and the OX_1 receptor involved in apoptosis are unknown.

In the earlier context described, the present work aims to investigate the role of each residue of orexin-B in the induction of apoptosis by the neuropeptide by using an 'alanine-scanning' strategy. Here, we showed that the C-terminus of orexin-B is crucial for the ability of the peptide to induce apoptosis. Based on the recent X-ray structure of the OX_2 receptor (Yin *et al.*, 2015), a 3D model of the OX_1 receptor was developed and used to design OX_1 receptor site-directed mutagenesis experiments, which demonstrated that seven specific residues are involved in the interaction of orexin-B with OX_1 receptors and in the ability of the peptide to induce a pro-apoptotic response. This study advances our knowledge on the molecular mechanism of the pro-apoptotic properties

of orexins, which is essential to design new agonists and/or biased agonists as novel therapeutic approaches for digestive and other types of cancers.

Methods

Stable expression of cDNA encoding human OX_1 and mutated OX_1 receptors in CHO-S cells

Full-length OX1R cDNAs were cloned into the expression vector pEYFP-N2 in fusion at the C-terminus with the yellow fluorescent protein as described previously (El Firar *et al.*, 2009). The plasmid encoding the human OX_1 receptor was stably transfected into CHO-S cells (ECACC 85050302) using X-tremeGENE (ROCHE Diagnostics, Meylan, France) according to the manufacturer's protocol. Transfected CHO-S cells were selected in the presence of 1 mg·mL^{-1} geneticin (G418, Life Technologies) for 2 weeks and cloned (Ceraudo *et al.*, 2008). OX_1 receptor mutants shown in Table 2 were obtained by site-directed mutagenesis as previously described (Ceraudo *et al.*, 2008). Each mutation was verified by sequencing. The recombinant mutants were stably expressed in CHO-S cells as described earlier.

Cell culture and radioreceptor assays

CHO-S cells expressing recombinant native or mutated OX_1 receptors were grown as previously described (El Firar *et al.*, 2009) and maintained at 37 °C in a humidified 5% CO_2/air incubator. [^{125}I]-orexin-A (74 TBq·mmol^{-1}) was prepared as previously described (El Firar *et al.*, 2009). Binding of [^{125}I]-orexin-A to subconfluent cells was conducted as described previously (El Firar *et al.*, 2009). It should be noted that orexin-A is used for this assay, as it contains a tyrosine residue that can be iodinated, which is not the case for orexin-B. Briefly, cells were incubated for 30 min at room temperature in 300 µL of 20 mM Tris/EDTA/saline binding buffer (pH 7.4) containing 0.5% (w v^{-1}) BSA, 5 mM KCL, 1 mM $CaCl_2$, 1.2 mM $MgCl_2$, 0.44 mM KH_2PO_4, 4.2 mM $NaHCO_3$, 10 mM glucose, 1 mM probenecid and 0.001% (v v^{-1}) Tween 20, in the presence of 0.25 nM [^{125}I]-orexin-Awith or without peptide analogues to be tested. Free peptides were removed by two cell washing cycles with PBS. The non-specific binding was determined in the presence of 1 or 10 µM unlabelled orexin-B and represented <5% of the total binding. All of the experiments were performed in triplicate and repeated at least three times.

Apoptosis and inositol phosphate assays

CHO-S cells expressing recombinant native or mutated OX_1 receptors were seeded and grown as described earlier. After 24 h of culture, cells were treated with or without peptide analogues to be tested at the concentration indicated in the figure legends. After 48 h of treatment, adherent cells were harvested by TryplE (Life Technologies). Apoptosis was determined using the Guava personal cell analysis system and the Guava nexin kit as previously described (Voisin *et al.*, 2008). Results are expressed as % of apoptotic annexin V-phycoerythrin-positive cells.

Subconfluent cells were labelled with [*myo*-^{3}H]-inositol (3.15 TBq·mmol^{-1}) (TRK883; GE Heathcare, Les Ullis, France) for 24 h in standard culture medium. Labelled cells were then incubated for 30 min at 37 °C in Tris/EDTA/saline binding buffer (pH 7.4) containing 20 mM lithium chloride with or without increasing concentrations of the peptide analogues to be tested. Cells were then treated with ice-cold formic acid, and total IP_3 was separated from free [*myo*-^{3}H]-inositol using column chromatography as previously reported (Rouet-Benzineb *et al.*, 2004).

Statistical analysis

Results are expressed as mean ± SEM. All statistical analyses were performed with GraphPad 4 (http://www.graphpad.com) The Mann–Whitney *U* test was used for comparison of mean values between two groups. Differences were considered statistically significant at $P < 0.05$.

Molecular modelling and molecular dynamics simulations

The model of the human OX_1 receptor (42–375) was built based on the 3D crystal structure of the human OX_2 receptor fusion protein to *Pyrococcus abysii* glycogen synthase bound to the insomnia drug suvorexant (Protein Data Bank ID code 4S0V) as template structure due to high sequence identity (64%) between the two types of receptor and using SWISS-MODEL (Arnold *et al.*, 2006; Benkert *et al.*, 2011; Biasini *et al.*, 2014). Protonation states of the titrable residues were assigned based on the pKa values calculated with the Propka server (www.poissonboltzmann.org). This model was embedded in a pre-equilibrated 1-palmitoyl-2-oleoyl-phosphatidylcholine (POPC) membrane model using CHARMM-GUI (Jo *et al.*, 2008; Wu *et al.*, 2014). Potassium and chloride ions were added to the system to a concentration of 150 mM. The final system contained 15 212 water molecules, 96 POPC lipid molecules, the OX_1 receptor model and ions with a simulation cell size of 66 × 66 × 152 Å. The system was first relaxed through energy minimization using the steepest descents algorithm. Then, an equilibration and production protocol included the following stages: (i) harmonic positional restrictions on all the heavy atoms of the receptor (five steps of 1 ns each, decreasing gradually the force constant from 1000 to 200 kJ·mol^{-1}·Å^{-2} in each step); (ii) harmonic positional restrictions on all backbone atoms of the receptor (4 ns); (iii) harmonic positional restrictions on all Cα atoms of the receptor (5 ns); and (iv) fully unrestrained simulations (100 ns). Docking simulations were performed using the NMR structure of the orexin-B C-terminus (pdb: 1CQ0). Briefly, the binding pocket of the structure of the OX_1 receptor at the end of the molecular dynamic (MD) simulation was determined using Fpocket webserver (Le Guilloux *et al.*, 2009). The largest pocket, localized at the top of the TM domains of the OX_1 receptor, was selected. The docking of the orexin-B C-terminus (sequence 20–28) into the OX_1 receptor was performed with Haddock webserver (http://haddocking.org). This model of the complex OX_1 receptor–orexin-B20–28 was then embedded in a pre-equilibrated POPC membrane model using CHARMM-GUI (Jo *et al.*, 2008; Wu *et al.*, 2014). Potassium and chloride ions were added to the system to a concentration of 150 mM. The final system contained 15

018 water molecules, 128 POPC lipid molecules, the model of the complex and ions with a simulation cell size of 75 × 75 × 130 Å. The system was first relaxed through energy minimization using the steepest descents algorithm. Then, an equilibration and production protocol included the following stages: (i) harmonic positional restrictions on all the backbone and side chains heavy atoms of the receptor and peptide (six steps, decreasing gradually the force constant from 4000 to 50 kJ·mol^{-1}·Å^{-2} for the backbone heavy atoms and from 2000 to 0 kJ·mol^{-1}·Å^{-2} for the side chain heavy atoms in each step for a total of 15 ns simulation time); and (ii) fully unrestrained simulations (100 ns).

Molecular dynamic simulations were performed with GROMACS 5.0 using the CHARMM22 protein force field with CMAP corrections (MacKerell *et al.*, 1998, 2004), the CHARMM36 lipid force field (Klauda *et al.*, 2010) and TIP3P water molecules. A semi-isotropic Parrinello–Rahman barostat was employed to maintain the pressure independently in the *x*-*y* plane and in the *z* direction at 100 kPa with a coupling constant of 5 ps. The isothermal compressibility constant was 4.5 × 10^{-5}·Pa^{-1}. The temperature was kept constant at 36.9 °C with the Nose–Hoover method and by coupling independently the lipid molecules, the protein and the water-ion groups with a common period of 1 ps. A cutoff of 1.2 nm was employed for the Lennard–Jones potential. The long-range interactions were calculated using the particle mesh Ewald method with a 1.2 nm real space cutoff, a 0.12 nm space grid and a fourth-order B-spline interpolation scheme to optimize the computational performance. The equations of motion were integrated using the leapfrog method with a 2 fs time step. The LINCS algorithm was used to constrain bond lengths in the protein and lipid molecules.

Molecular dynamic trajectories analyses were conducted using GROMACS utilities. All the calculations were performed with the supercomputing resources available at the Centre de Calcul Recherche et Technologie (CEA, France). Three-dimensional representations of the interaction between the C-terminal region of orexin-B and the 3D model of the OX_1 receptor were drawn using Chimera software (http://www.cgl.ucsf.edu/chimera/).

Materials

Enzymes, vectors and culture medium were obtained from Life Technologies (Saint Aubin, France). All orexin-B analogues were obtained by custom solid-phase synthesis from GL Biochem (Shanghai, China), and all were at least 95% pure. [^{125}I]-orexin-Awas prepared and purified as previously described (Voisin *et al.*, 2008). All other highly purified chemicals were from Sigma-Aldrich (Saint Quentin-Fallavier, France).

Results

Structure–function relationship of orexin-B

Previous reports have clearly demonstrated that orexin-A and orexin-B induce mitochondrial apoptosis in colonic cancer cell lines as HT-29, LoVo and other cell lines, which express OX_1 but not OX receptors (Voisin *et al.*, 2011). In order to identify the pharmacophore of orexin-B responsible for this effect, we used the alanine scanning technique (Nicole *et al.*, 2000). Twenty-five mutants of orexin-B were synthesized in which the 25 residue side chains were individually replaced with alanine. As the residues in position 17, 22 or 23 of the native peptide are alanine, three additional mutants were synthesized, substituting the alanine for a leucine residue. All mutants were tested for their interaction with human recombinant OX_1 receptor, stably expressed in CHO-S cells, by competitive inhibition of [^{125}I]-orexin-A binding. The slopes of the mutant dose–response curves for inhibiting [^{125}I]-orexin-A binding were identical for all mutants (not shown). All competitor curves analysed with the GraphPad software fitted to a monophasic binding pattern, indicating the presence of only one binding site (Supporting Information Figures S1B and S2B). When the IC_{50} of all mutants was analysed, the largest decrease in affinity for the OX_1 receptor occurred when A^{22}, G^{24}, I^{25}, L^{26} and M^{28} were substituted for alanine or leucine, resulting in a 40-fold to 200-fold decrease (Table 1, Figure 1 and Supporting Information Figure S2B). Alanine substitution of L^{11} and L^{15} resulted in significant decrease in IC_{50} but by only 10-fold (Table 1, Figure 1 and Supporting Information Fig. S2A). It should be noted that alanine substitutions at positions 20 and 27 induced a significant weak decrease in affinity, that was, lesser than fivefold. Substitution at other positions, including S^{18}, N^{20} and T^{27}, did not change the affinity or resulted only in decreases of less than one log (Table 1 and Figure 1).

All orexin-B mutants were tested for their ability to stimulate IP_3 production in CHO-S–OX_1 receptor cells (Table 1). The dose–response curves of IP_3 production for all mutants were identical to those of native orexin-B (Supporting Information Fig. S1A and B). There was a good correlation between the EC_{50} for intracellular IP_3 production and the IC_{50} for the binding inhibition of [^{125}I]-orexin-A to OX_1 receptors (Table 1). A straight line (r = 0.92) was obtained when plotting logEC_{50} versus logIC_{50}, indicating that all mutants behaved as OX_1 receptor agonists, with identical or lower potencies than native orexin-B (Figure 2). Taken together, these data demonstrate the importance of five crucial residues in the C-terminal sequence of orexin-B, that is, A^{22}, G^{24}, I^{25}, L^{26} and M^{28} (Figure 1, Supporting Information Fig. S1A and B). Nevertheless, a minor contribution of the central part of the peptide is also to be noted, specifically the L^{11} and L^{15} residues (Table 1, Figure 1 and Supporting Information Fig. S1A). All mutants were then tested for their ability to trigger apoptosis in CHO-S–OX_1 receptor cells. As expected, alanine substitution of L^{11}, L^{15}, A^{22}, G^{24}, I^{25}, L^{26} and M^{28}, which all played a role in orexin-B affinity and cellular IP_3 production (see preceding text), decreased peptide-induced apoptosis by 50-fold to 500-fold (Table 1, Figure 1, Supporting Information Figs S1A and B).

Interestingly, a strong decrease in the ability to induce apoptosis occurred when S^{18}, N^{20} and T^{27} were substituted for alanine (Table 1 and Figure 1). Indeed, these substitutions produced at least a 100-fold drop in orexin-B-induced apoptosis (Table 1 and Figure 1), even though they were able to bind to OX_1 receptors with relatively good affinity (Table 1 and Figure 1). Similarly, although to a lesser extent, mutants Q16A and A17L, which bind to the OX_1 receptor with a similar affinity as wild-type (wt) orexin-B, exhibited a

Table 1

Biological activity of orexin-B mutants in CHO-S cells stably expressing human recombinant OX_1 receptors (OX1R)

Orexin-B residues	Substitution	Binding affinity IC_{50} (nM)	IP_3 production EC_{50} (nM)	Apoptosis induction EC_{50} (nM)
wt	–	31.2 ± 1.4	28.0 ± 5.8	19.6 ± 2.1
R1	Ala	34.4 ± 2.7	51.0 ± 6.7*	10.9 ± 0.9*
S2	Ala	51.0 ± 6.7*	63.0 ± 49.6	30.3 ± 10.2
G3	Ala	27.3 ± 2.2	14.0 ± 4.9	24.7 ± 4.1
P4	Ala	34.3 ± 2.7	8.8 ± 5.6	21.1 ± 2.8
P5	Ala	5.5 ± 0.8*	10.8 ± 3.5	29.1 ± 7.0
G6	Ala	46.7 ± 3.4*	96.3 ± 18.2*	33.9 ± 5.9
L7	Ala	33.4 ± 8.3	32.2 ± 4.3	24.2 ± 4.6
Q8	Ala	9.3 ± 0.7*	8.1 ± 1.1*	24.7 ±4.1
G9	Ala	46.1 ± 11.2	38.7 ± 11.4	50.2 ± 10.8
R10	Ala	34.3 ± 2.7	14.2 ± 3.0	27.3 ± 2.2
L11	Ala	300.1 ± 48.9*	360.6 ± 136.0*	1109.5 ± 475.5*
Q12	Ala	23.4 ± 1.7*	6.7 ± 3.0*	26.0 ± 7.1
R13	Ala	32.2 ± 4.3	13.2 ± 2.6	20.3 ± 2.7
L14	Ala	21.4 ± 5.5	14.0 ± 4.1	21.5 ± 2.4
L15	Ala	375.1 ± 63.1*	105.8 ± 26.4*	3223.5 ± 1763.9*
Q16	Ala	29.4 ± 2.2	30.0 ± 4.9	368.6 ± 138.9*
A17	Leu	34.3 ± 2.7	31.6 ± 2.3	491.6 ± 258.3*
S18	Ala	20.7 ± 0.8*	43.9 ± 6.2	5987.3 ± 2006.3*
G19	Ala	29.4 ± 2.2	12.5 ±4.3	26.9 ± 7.0
N20	Ala	157 ± 39*	238.4 ±79.9*	>10 000
H21	Ala	30.5 ± 1.1	23.9 ± 3.9	106.0 ± 4.9*
A22	Leu	3491 ± 490*	>10 000	7504 ± 111.4*
A23	Leu	10.9 ± 0.9*	18.4 ± 0.9	64.8 ± 12.0*
G24	Ala	3982.3 ± 820.3*	>10 000*	7733.3 ± 2266.7*
I25	Ala	6674 ± 1663*	>10 000*	3799.3 ± 1133.5*
L26	Ala	3563.7 ± 236.6*	>10 000*	>10 000*
T27	Ala	215.6 ± 70.4*	142.4 ± 58.6*	>10 000*
M28	Ala	1263 ± 370.8*	317.3 ± 93.2*	7333.3 ± 2666.7*
OxB6–28	–	47.4 ± 8.9	81.7 ± 24.9*	75.1 ± 20.4*
OxB7–28	–	388.0 ± 112.5*	1513.7 ± 255.4*	2183.0 ± 1133.6*
S18, N20	Ala, Ala	200.2 ± 58.8*	>10 000*	>10 000*
S18, T27	Ala, Ala	175.0 ± 24.5*	>10 000*	>10 000*

IC_{50} for inhibition of [^{125}I]-orexin-A binding and EC_{50} for stimulation of IP_3 production or apoptosis induction. All parameters were determined in CHO-S–OX1R cells. Data are mean ± SEM of at least three experiments performed in triplicate. wt, wild type. *$P < 0.05$, significantly different from wt.

decrease in pro-apoptotic activity by about 20-fold (Table 1). Globally, a good correlation (r = 0.80) between the EC_{50} for induction of apoptosis and IC_{50} for inhibiting [^{125}I]-orexin-A binding was observed for all mutants, except for the S18A, N20A and T27A mutants (Figure 2), suggesting that these peptides behaved as partial OX_1 receptor agonists. When they were omitted from the regression curve, the correlation coefficient improved (r = 0.90), indicating a lack of correlation between OX_1 receptor affinity and apoptosis induction for the S18A, N20A and T27A mutants.

To confirm these observations, two new orexin-B mutants were synthesized with double substitution by alanine of the S^{18} and N^{20} or S^{18} and T^{27} residues. As shown in Table 1 and Figure 3A, both double mutants slightly altered the ability

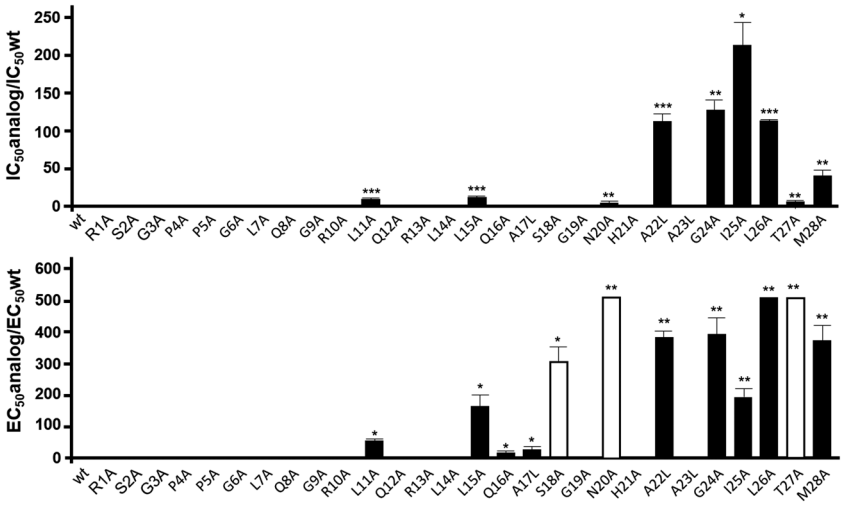

Figure 1

Binding characteristics (top panel) and pro-apoptotic properties (bottom panel) of wt human orexin-B and peptide analogues. Single amino acids in the wt orexin-B sequence were replaced by L-alanine or L-leucine as shown ont the *x*-axis. Top panel: wt OX_1 receptors were stably expressed in CHO-S cells, and competitive inhibition of [^{125}I]-orexin-A binding by unlabelled mutants was analysed. The concentration of each mutant that half maximally inhibited specific [^{125}I]-orexin-A binding (IC_{50}) was determined and the ratio IC_{50}mutant/IC_{50}wt was calculated; Bottom panel: pro-apoptotic activity of wt orexin-B and peptide analogues determined in CHO-S–OX_1 receptor cells. The concentration of each mutant that half maximally induced cellular apoptosis (EC_{50}) was determined and the ratio EC_{50}mutant/EC_{50}wt was calculated. $^{*}P < 0.05$, $^{**}P < 0.001$, $^{***}P < 0.0001$.

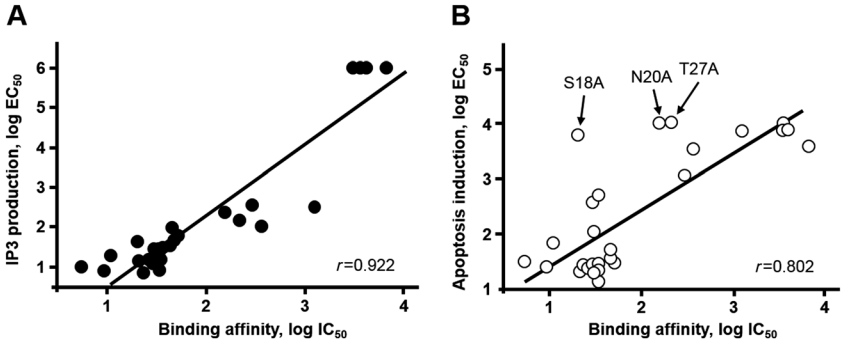

Figure 2

Correlation between the EC_{50} values and IC_{50} values determined for native orexin-B and all singly substituted mutants of orexin-B. (A) Correlation between the EC_{50} values and K_i values determined for the IP_3 and binding assays in CHO-S cells stably expressing recombinant OX_1 receptors (CHO-S–OX1R). (B) Correlation between the EC_{50} values and IC_{50} values determined for the apoptosis and binding assays in CHO-S–OX1R. Note the S18A, N20A and T27A mutants for which the EC_{50} for inducing cellular apoptosis was much higher than their IC_{50} for binding. See Table 1 for details.

of the peptide to interact with the OX_1 receptor (IC_{50} = 31.2 nM for wt versus 200.2 nM for S18A/N20A and 175 nM for S18A/T27A). In contrast, both strongly abolished the production of IP_3 and the induction of apoptosis (Table 1). Thus, these data suggest that the S18A/N20A and S18A/T27A mutants might be partial agonists. To confirm this, the ability of orexin-B to inhibit cell growth was measured in the presence or absence of either the S18A/N20A or S18A/T27A peptides. As shown in Figure 3, orexin-B induced a strong inhibition of cell growth in a dose-dependent manner, with an EC_{50} of about 25 nM. Addition of various concentrations (0.1 to 10 μM) of mutants partially inhibited the orexin-B-induced inhibition of cell growth. Indeed, addition of 10 μM of S18A/N20A or S18A/T27A peptides totally abolished the response induced by 0.1 nM orexin-B (Figure 3C and D), whereas both mutants partially antagonized the effect of 1 to 10 μM orexin-B. Schild plots (Arunlakshana and Schild, 1959) derived from these experiments indicated that the regression line slope was about 0.85 for both analogues (Supporting Information Fig. S2), which is not significantly different from 1, suggesting that the mutants are competitive antagonists. These results indicate that the double mutant S18A/N20A and S18A/T27A peptides are partial agonists for apoptosis induction.

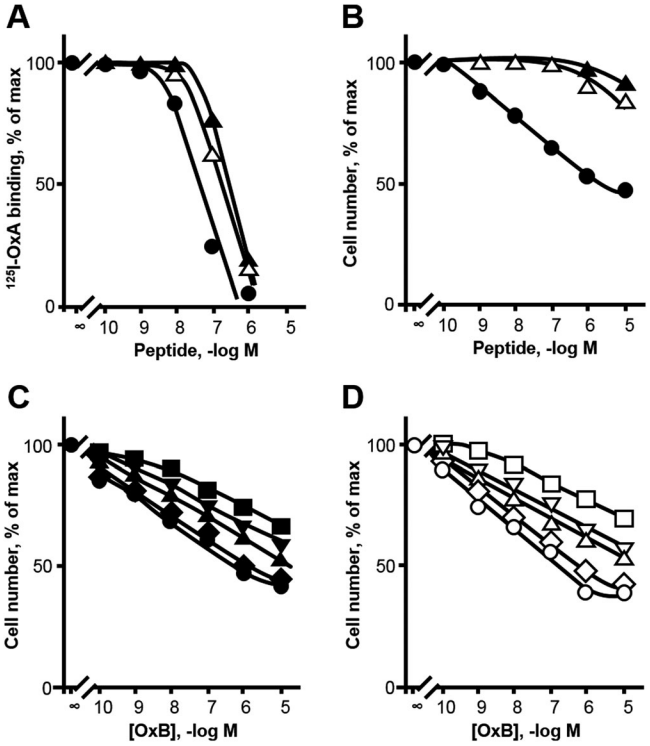

Figure 3

Specific [^{125}I]-orexin-A (OxA) binding to CHO-S–OX$_1$ receptor (OX1R) cells in the presence of increasing concentrations of unlabelled orexin-B, S18A/N20A and S18A/T27A peptides (A) and determination of the inhibition of cellular growth induced by increasing concentrations of orexin-B, S18A/N20A (B, C) and S18A/T27A (B, D) peptides in CHO-S–OX1R cells. (A) CHO-S–OX1R cells were incubated with the indicated concentrations of orexin-B, S18A/N20A and S18A/T27A. Results are expressed as % of radioactivity specifically bound in the absence of added unlabelled peptide. (B) CHO-S–OX1R cells were incubated with the indicated concentrations of orexin-B, S18A/N20A and S18A/T27A, and cells were counted after 48 h incubation. Results are expressed as % of total viable cells. (C, D) Increasing concentrations of orexin-B were incubated together with the following concentrations of S18A/N20A mutant (C): 0, 10 nM, 100 nM, 1 μM, 10 μM, or S18A/T27A mutant (D). Each point is the mean of three separate experiments. For clarity, SEM are not indicated; they were always below 15% of mean values.

In order to determine the minimal sequence of orexin-B having a full biological activity, two deletion mutants were also synthesized (Table 1). Deletion of the first five residues of orexin-B (orexin-B6–28) did not alter the peptide's ability to inhibit the binding of [^{125}I]-orexin-A to the OX$_1$ receptor as compared with native orexin-B (Table 1). In contrast, deletion of the first six residues (orexin-B7–28) induced a decrease in affinity for OX$_1$ receptors (Table 1) by more than one log. Orexin-B6–28 induced apoptosis and IP$_3$ production similarly to wt orexin-B (Table 1), while orexin-B7–28 strongly altered peptide-induced apoptosis and IP$_3$ production (Table 1). Taken together, these data suggest that the peptide must be at least 22-aminoacids long to induce these responses.

A 3D model of the OX$_1$ receptor and docking of the orexin-B C-terminus

Based on the high degree of sequence identity between human OX$_1$ and OX$_2$ receptor (64%), the crystallographic structure of the OX$_2$ receptor was employed as a template to generate a homology model of the OX$_1$ receptor. This model was employed as a starting conformation for an all-atom MD simulation in a lipid bilayer. After 100 ns MD production, the model was comparable with OX$_2$ receptor structure with the backbone root mean square deviation (RMSD) value of 1.02 Å between the OX$_1$ receptor model and OX$_2$ receptor structure. The OX$_1$ receptor 3D model exhibited one short helix in the intracellular C-terminal tail (G^{363} to S^{374}, Figure 4), as observed in the structure of the OX$_2$ receptor (Yin *et al.*, 2015). The orexin-B C-terminus (sequence 20–28) was then docked into the structure of OX$_1$ recepto obtained at the end of the 100 ns MD production. Among the various docking poses obtained, one 3D model was selected on the basis of best score (−112.7 ± 6.8), maximal buried surface area (1492 Å ± 58.8) and spatial orientation of the orexin-B20–28 C-terminus (Figure 4). Indeed, the model shows that the C-terminal M^{28} residue of the orexin-B20–28 peptide is located well inside the binding pocket, whereas the N-terminal N^{20} residue is oriented outside of the pocket. The complex OX$_1$ receptor/orexin-B20–28 was embedded into a membrane, and the resulting system was submitted to MD simulation (see Supporting Information Fig. S3, which depicts a side view of the simulated system). The global fold of the complex is stable during the production as shown by the values of the RMSDs (Supporting Information Fig. S4). Indeed, the backbone RMSD of the TM domains (Supporting Information Fig. S4), the interface helix (amino acids 363–372) (Supporting Information Fig. S5) and the ß-sheet (amino acids 183–204) (Supporting Information Fig. S5) of the OX$_1$ receptor fluctuate, as a function of time, between 0.5 and 2 Å, except for TM5 in the complex. In fact, the C-terminus of TM5 slightly unwound during the last 50 ns of the simulation. Figure 4 depicts the C-terminus of orexin-B inserted into the binding pocket delineated by all the TM domains of the OX$_1$ receptor except TM1. Most of orexin-B contacts involve van der Waals interactions and some hydrogen bonds (from Y^{224} OH group to backbone carbonyl of T^{27} and from N^{318} NH2 group to backbone carbonyl of G^{24}) (Figure 5). In contrast, one ionic bond was identified between K^{120} and E^{184}, one hydrogen bond between W^{145} and the backbone carbonyl of A^{52} and one hydrogen bond between T^{341} and the backbone carbonyl of A^{338} (Figure 5). It should be noted that the orexin-B20–28 peptide inserted into the OX$_1$ receptor adopts a helical conformation for residues H^{21} to T^{27} (Supporting Information Fig. S6).

Site-directed mutagenesis analysis of the receptor

Based on the distance measured between the side-chain residues of the OX$_1$ receptor TM domains and those of the orexin-B20–28 peptide, we selected residues within the OX$_1$ receptor-TMs and orexin-B20–28. All residues of the OX$_1$ receptor fulfilling this condition were mutated to alanine by site-directed mutagenesis (Table 2 and Figure 5). All mutants were functionally expressed in CHO-S cells (not shown) and tested for their abilities to bind [^{125}I]-orexin-A and to induce

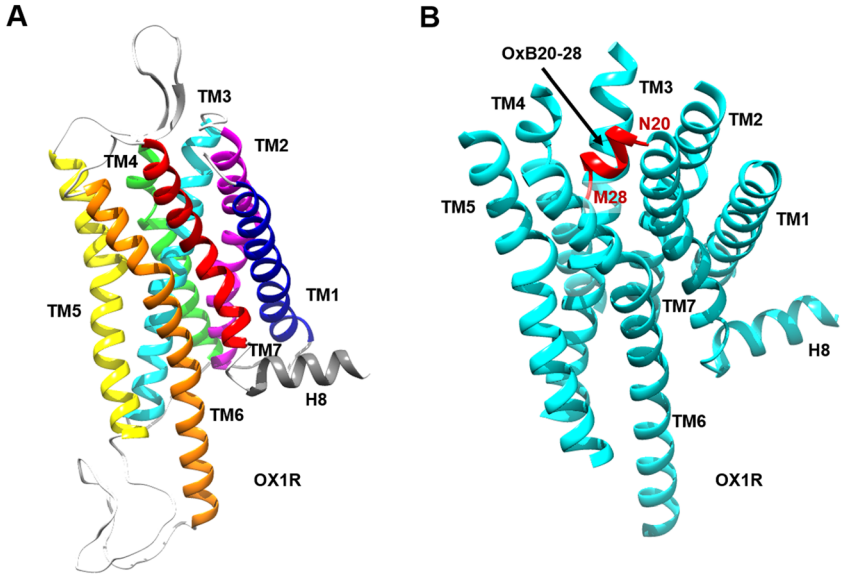

Figure 4

Representation of the 3D model of the OX_1 receptor (OX1R) receptor (A) docked to the C-terminus of orexin-B (OxB; B). (A) 3D model of human OX1R based on X-ray structure of OX2R. TM domains 1 to 7 are coloured dark blue, purple, turquoise, light green, yellow, orange and red respectively. (B) 3D model of human OX1R (turquoise) docked to sequence 20–28 of orexin-B (red). Intracellular loops and ECLs are not represented.

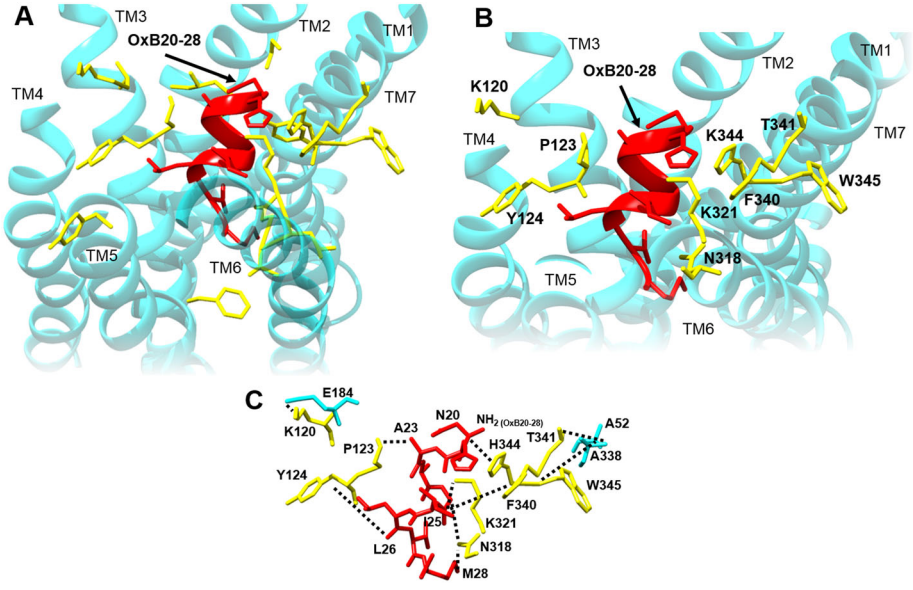

Figure 5

Upside-down view of the 3D model of human OX_1 receptor (OX1R) docked to the C-terminus of orexin-B (OxB). (A) Side chains of residues (yellow sticks) of the receptor 3D model (turquoise) in the surroundings of sequence 20–28 of orexin-B (red). All the represented residues (yellow sticks) were substituted to alanine. (B) 3D model of human OX1R (turquoise) docked to the C-terminus of orexin-B (red). OX1R residues for which the alanine substitution resulted in an inhibition of the ability of orexin-B to bind to the receptor and to induce cellular apoptosis are indicated (yellow). (C) Putative interactions (ionic and van der Walls) between residues of OX1R (yellow), which were mutated and residues of orexin-B (red). Residues in turquoise represent native OX1R residues.

apoptosis response, as mentioned above (Table 2). Mutants I98A, C99A, P101A, V121A, Y211A, F220A, V319A, L320A, K321A and Y348A were able to bind [^{125}I]-orexin-A and to induce apoptosis with an IC_{50} in the nm range, which is similar to the IC_{50} determined for the wt OX_1 receptor, for example, $IC_{50}mut/IC_{50}wt < 5$ and $EC_{50mut}/EC_{50wt} < 5$ (Table 2

Table 2

Site-directed mutagenesis of OX_1 receptors (OX1R)

Mutants	Localization	Binding affinity IC_{50} (nM)	IC_{50}mut/IC_{50}wt	Apoptosis induction EC_{50} (nM)	EC_{50}mut/EC_{50}wt
wt	–	29.0 ± 5.2	1.0	28.3 ± 4.8	1.0
I98A	TM2	41.4 ± 2.1*	1.4	11.4 ± 0.7*	0.4
C99A	TM2	58.6 ± 12.0*	2.0	31.2 ± 5.2	1.1
P101A	TM2	58.1 ± 2.1*	2.0	111.4 ± 10.8*	3.9
K120A	TM3	>10 000	>400	>10 000	>400
V121A	TM3	52.1 ± 11.6*	1.8	78.1 ± 12.4*	2.8
P123A	TM3	>10 000	>400	>10 000	>400
Y124A	TM3	408.2 ± 73.5*	14.0	295.0 ± 68.4*	10.5
Y211A	TM5	20.9 ± 0.9	2.3	35.5 ± 5.7	1.3
F220A	TM5	21.4 ± 4.2	0.7	17.5 ± 3.8	0.6
N318A	TM6	165.6 ± 44.7*	5.7	151.1 ± 22.3*	5.3
V319A	TM6	24.8 ± 3.1	0.9	33.5 ± 6.2	1.2
L320A	TM6	51.4 ± 17.8	1.8	17.5 ± 4.7	0.6
K321A	TM6	132.5 ± 23.2*	15.0	71.8 ± 16.2*	2.5
F340A	TM7	700 ± 74.9*	24.0	517.5 ± 42.6*	18.0
T341A	TM7	358.1 ± 120.2*	12.0	261.5 ± 58.2*	9.0
H344A	TM7	>10 000	>400	>10 000	>400
W345A	TM7	2094.8 ± 88.5*	72.0	1792.6 ± 74.5*	64.0
Y348A	TM7	37.2 ± 5.8	1.2	151.5 ± 28.9*	5.4

IC_{50} for inhibition of [^{125}I]-orexin-A binding and EC_{50} for apoptosis induction. All parameters were determined in CHO-S cells stably expressing human recombinant OX1R. Data are mean ± SEM of at least three experiments performed in triplicate. wt, wild type. *$P < 0.05$, significantly different from wt.

and Figure 5). Of note, the substitution of Y^{348} by an alanine residue induced a slight inhibition of the OX_1 receptor interaction with the peptide ligand and of apoptosis (Table 2). Inversely, the K321A mutant has altered binding parameters, whereas its ability to induce apoptosis was similar to the wt OX_1 receptor (Table 2). The Y124A, N318A, F340A and T341A mutants displayed much lower affinity for [^{125}I]-orexin-A than the wt OX_1 receptor with a ratio IC_{50}mut/IC_{50}wt < 25 (Table 2). As shown in Table 2, these mutants inhibited apoptosis, with a ratio EC_{50}mut/EC_{50}wt < 25. It should be noted that the IC_{50} for [^{125}I]-orexin-A binding for these mutants was very similar to the EC_{50} determined for the apoptosis response (Table 2). However, substitution of K^{120}, P^{123}, H^{344} and W^{345} residues by an alanine residue had a strong impact on receptor affinity and the apoptotic response (Table 2 and Figure 5), indicating that these residues play a critical role in the interaction of OX_1 receptors with orexins and/or the structure of the OX_1 receptor. Indeed, the Y124A, F340A and T341A mutants displayed a ratio IC_{50}mut/IC_{50}wt > 10 and EC_{50}mut/EC_{50}wt > 10 (Table 2), the W345A mutant displayed a ratio IC_{50}mut/IC_{50}wt > 60 and EC_{50}mut/EC_{50}wt > 60 (Table 2), whereas the K120A, P123A and H344A mutants displayed a ratio IC_{50}mut/IC_{50}wt > 400 and EC_{50}mut/EC_{50}wt > 400.

Discussion and conclusion

Several studies in recent years have shown that GPCRs represent new promising targets for the therapeutic treatment of various cancers (Lappano and Maggiolini, 2011). Among the large GPCR family, the OX receptors, a class A GPCR expressed in the hypothalamus, also display pro-apoptotic properties in cancer cell lines (Laburthe and Voisin, 2012). Our group demonstrated in the last few years that the OX_1 receptor is not expressed in normal colon tissue but is ectopically expressed in colon cancers where orexins bound to OX_1 receptors induce: (i) robust mitochondrial apoptosis (El Firar *et al.*, 2009); and (ii) significant inhibition of tumour growth in nude mice xenografted with cancer cell lines (Voisin *et al.*, 2011). These effects are mediated via a novel mechanism involving (i) the presence of two ITIM sequences in the OX_1 receptor that are tyrosine phosphorylated upon receptor binding of orexins (Voisin *et al.*, 2008); and (ii) the recruitment to tyrosine phosphorylated sites and activation of the tyrosine phosphatase, SHP-2, which is responsible for mitochondrial apoptosis involving cytochrome c release from mitochondria to cytosol and caspase-3 and caspase-7 activation (El Firar *et al.*, 2009). In this context, the determination of the pharmacophore involved in the pro-apoptotic

properties of the orexin peptide represents a key step for the design of new molecules with therapeutic interest. Although some studies regarding the pharmacophore determination of orexins to mobilize intracellular Ca^{2+} have been reported (Darker *et al.*, 2001; Lang *et al.*, 2004; German *et al.*, 2013; Heifetz *et al.*, 2013), no systematic evaluation of the pro-apoptotic function of every residue of orexin-B has been performed. In the present study, we have synthesized a total of 28 single alanine or leucine mutants of orexin-B and have analysed their biological properties by binding assay, ability to stimulate intracellular IP_3, and thereby Ca^{2+} release, and cellular apoptosis measurements in CHO-S cell clones expressing recombinant human OX_1 receptors. Our data provide critical new information on the key orexin-B amino acid residues that play a role in the pro-apoptotic function of the peptide.

Analysis of the 28 single alanine or leucine substitutions indicated that 12 residues in native orexin-B could not be changed without a significant decrease either in (i) the binding affinity for the OX_1 receptor; (ii) the ability to stimulate IP_3 production; or (iii) the ability to induce a pro-apoptotic response in transfected cells. These important residues were distributed mainly at the C-terminal end of the peptide chain, except for L^{11} and L^{15}, which are located in the peptide middle region. These results are in good agreement with previous observations indicating that the C-terminal end of orexin-B is crucial for both the binding to the OX_1 receptor and the mobilization of intracellular Ca^{2+} (Lang *et al.*, 2004). Moreover, the deletion of the first five residues of orexin-B had no impact on the ability of the truncated peptide to bind to OX_1 receptors, induce IP_3 production and trigger cellular apoptosis. In contrast, the deletion of one more residue (orexin-B7–28) strongly reduced the peptide activity, suggesting that the sequence 6–28 is essential for peptide function. Thus, we identified seven residues, that is, L^{11}, L^{15}, A^{22}, G^{24}, I^{25}, L^{26} and M^{28}, as critical for binding to human OX_1 receptors and subsequent induction of cell apoptosis. It is quite interesting to note that all these residues in orexin-B are conserved in orexin-A, except for M^{28}, which is a homolog to L^{33} in orexin-A. Moreover, the analysis of the side chain of these residues indicated mainly the presence of hydrophobic residues (L^{11}, L^{15}, A^{22}, G^{24}, and I^{25} and L^{26}) and also the presence of one non-polar residue (M^{28}). Inversely, the substitution to alanine or leucine of the Q^{16}, A^{17}, S^{18}, N^{20} and T^{27} residues had only a weak impact on binding affinity and Ca^{2+} mobilization, although it affected the induction of apoptosis. The structure determination of orexin-B by NMR had previously revealed the presence of two α-helices at position L^7–G^{19} (Helix I) and A^{23}–M^{28} (Helix II), connected by a flexible loop (Lee *et al.*, 1999). Residues S^{18} and N^{20} are located in the flexible loop, while T^{27} is found in Helix II. Alanine substitution of S^{18}, N^{20} and T^{27} strongly abolished peptide-induced apoptosis in CHO-S–OX_1 receptors, but the ability of these mutants to bind OX_1 receptors was not affected by alanine substitution of S^{18} and only slightly affected by alanine substitution of the N^{20} and T^{27} residues. These observations suggest that these three residues might play a key role in the induction of apoptosis mediated by orexins binding to their cognate receptors. The double substituted S18A/N20A and S18A/T27A peptides exhibited a slightly altered ability to interact with OX_1 receptors, indicating that substituting two of the three critical residues do not substantially alter affinity compared with single substitution of N^{20} and T^{27} residues. Although the possibility that the double substitutions have a structural impact on orexin-B molecules cannot be excluded. Moreover, these double substitutions totally abolished the ability of the two peptides to induce cellular apoptosis, suggesting that these peptides could be partial agonists/antagonists. Indeed, these two peptides partially antagonized the inhibition of cellular growth by orexin-B through a competitive mechanism. Thus, both the flexible loop and the C-terminal Helix II play a crucial role in the peptide main activity.

Sequence analysis of class A GPCRs revealed that there is a large diversity in the length and residue composition of the extracellular loops (ECLs). ECLs, and more particularly ECL2, which links TM4 and TM5, displayed different structures, including helices (e.g. in some aminergic or adenosine receptors) or β-sheets (e.g. peptide-binding receptor) (Venkatakrishnan *et al.*, 2013). A unique feature of the extracellular region of class A GPCRs is the presence of a disulfide bridge between a cysteine residue located in TM3 and a cysteine residue located in ECL2 (Fanelli and De Benedetti, 2011). The disulfide bridge has been shown to be involved in GPCR stability and activity (De Graaf *et al.*, 2008). Indeed, the TM3-ECL2 disulfide bridge stabilized the extracellular side of TM3 close to the binding pocket and limited the conformational change of this region during receptor activation (Preininger *et al.*, 2013). The recent determination of the structure of the OX_2 receptor (Yin *et al.*, 2015), which shares 64% sequence identity with the OX_1 receptor, allowed us to develop a homology 3D model of the OX_1 receptor that was subsequently used for ligand docking studies. The use of GPCR models in combination with site-directed mutagenesis represents an effective tool to study both ligand binding and functional properties. The OX_1 receptor model exhibited an eighth helix (H8) at the top of the C-terminal sequence between residues G^{363} and S^{374}. The existence of H8 is frequently observed in class A GPCRs, except for the CXCR4, NTS_1 receptor and PAR1 in which this region is unstructured (Venkatakrishnan *et al.*, 2013). The structural and/or functional role of H8 in GPCRs remains conjectural, although some reports indicated a role in coupling and activation of G proteins (Rasmussen *et al.*, 2011a).

As mentioned earlier, the C-terminal end of orexin-B had a crucial role not only in the binding activity of the peptide but also in its ability to induce a pro-apoptotic response. To understand how the C-terminal helix of orexin-B interacts with OX_1 receptor, we docked the C-terminal 20–28 fragment of orexin-B into the homology model of the OX_1 receptor. We substituted independently to alanine 18 residues of the OX_1 receptor (Table 2), and showed that the substitution of nine of these residues (K^{120}, P^{123}, Y^{124}, N^{318}, K^{321}, F^{340}, T^{341}, H^{344} and W^{345}), located in the TM2, TM3, TM6 and TM7 of the OX_1 receptor, reduces the binding affinity of orexin-B to the OX_1 receptor and inhibits the ability of orexin-B to induce apoptosis. OX_1 receptor/orexin-B20–28 complex model analysis has shown that most of these residues were located close to orexin-B20–28. Indeed, P^{123} was close to A^{22}, Y^{124} close to L^{26}, N^{318} close to G^{24}, K^{321} close to I^{25}, F^{340} close to I^{25} and H^{344} close to N^{20} (Figure 5) suggesting that these residues could be involved in the interaction between the OX_1

receptor and its ligand. In contrast, K^{120}, T^{341} and W^{345} were clearly far from orexin-B20–28 residues suggesting that these residues were involved in the structural maintaining of the receptor (Figure 5). Alanine substitution of P^{123} and H^{344} resulted in a strong reduction of the ability of the receptor to bind orexin-B and to trigger an apoptotic response. These residues are located in TM3 and TM7 of OX1R and delineated the binding pocket. Based on homology modelling of the OX_1 receptor using the human dopamine D_3 receptor as a template, Heifetz *et al*. (2013) have demonstrated the important role of OX_1 receptor residues in the ability of orexin-B to mobilize intracellular calcium including D^{203}, W^{206}, Y^{215}, F^{219}, Y^{224}, Y^{311} and H^{344}. As shown in this study, the prediction of 2D interaction map suggested that H^{344} was in interaction of L^{11} and L^{15} located in Helix I of orexin-B (Heifetz *et al*., 2013). This prediction totally contrasted with the present data indicating that H^{344} interacted with N20 of orexin-B. These observed differences could be caused by the differences between the OX_1 receptor 3D models used. The determination of X-ray structure of the OX_2 receptor in the presence of the dual orexin receptor antagonist, suvorexant, revealed that it lodged deep in the orthosteric site and contacted all TM domains except TM1 (Yin *et al*., 2015). Analysis of the OX_2 receptor binding pocket reveals that N^{324} and H^{350} were in direct contact with suvorexant (Yin *et al*., 2015). These data suggested that the corresponding residues in the OX_1 receptor, that is, N^{318} and H^{344} could play a direct role in the interaction of orexin-B with the OX_1 receptor. Assuming that the alanine substitution of H^{344} strongly abolished the ability of the OX_1 receptor to recognize orexin-B and to induce the pro-apoptotic response, this residue was one of the key residues involved in the activity of the OX_1 receptor. A previous report had revealed that substitution of residue Y^{348} did not modify the ability of the OX_1 receptor to bind orexin-A and to mobilize intracellular calcium (Heifetz *et al*., 2013). In this study, the substitution of Y^{348} induced only a weak alteration of OX_1 receptor affinity and its ability to induce cellular apoptosis. However, the 2D interaction map of contact between the antagonist suvorexant and the OX_2 receptor revealed that Y^{354} (corresponding to Y^{348} in OX_1 receptor) is in contact with the ligand (Yin *et al*., 2015). The same observation was obtained for the OX_2 receptor P^{131} residue (corresponding to P^{123} in OX_1 receptor), indicating that OX_1 receptor residues P^{123} and to a lesser extent Y^{348} could directly interact with orexin-B. Finally, a hypothetic 3D model of the complex OX_1 receptor/orexin-B has been constructed by structural alignment of the docked orexin-B20–28 with full sequence of orexin-B (Supporting Information Fig. S7). The resulting model showed that the Helix I of orexin-B was mainly located along the partially β-sheet structured ECL2, which could act as an anchorage site for L^{11} and L^{15} located in the middle part of orexin-B.

As mentioned earlier, the orexins/OX_1 receptor complexes have pro-apoptotic properties mediated by SHP-2 recruitment via phosphorylation of tyrosine residues (Y^{83} and Y^{358}) located in TM2 and TM7 (Laburthe and Voisin, 2012). This mechanism accounted for the dual participation of the Gq β/γ dimer and OX_1 receptor ITIM sites (Laburthe and Voisin, 2012). Agonist-mediated activation of the GPCRs involved inward movements of TM5 and TM6 relative to the rest of TM bundle as observed for the β_2 adrenoceptor (Rasmussen *et al*., 2011b) and M_2 (muscarinic) acetylcholine receptor (Kruse *et al*., 2013). Moreover, it was demonstrated that the binding of agonist peptide to the GPCR promoted the conformational change inducing a destabilization of the inactive state and a stabilization of the active state, leading in the case of the OX_1 receptor to the production of IP_3 and recruitment of SHP-2. Recent data indicated that the orexin-B and also orexin-A peptides binding altered noncovalent interactions between TM3 and TM6 leading to a decrease in the stability of the inactive state of the receptor (Heifetz *et al*., 2013). In the present work, orexin-B and OX_1 receptor mutants, which modified their activities in terms of binding, production of IP_3 and stimulation of the apoptosis, probably altered the ability to destabilize the inactive state of the receptor. In contrast, orexin-B mutants S18A, N20A and T27A, which were only altered in their abilities to induce apoptosis, partially promoted the active state but did not interact with the transmission switch residues located in the TM domain and involved in the unmasking of tyrosine residues responsible for SHP-2 recruitment.

Conclusions

The present 'Ala-scan' study of orexin-B, associated with the development of a global 3D model of the OX_1 receptor and site-directed mutagenesis, demonstrated that the C-terminal end of orexin-B and seven residues located in the TM domains of the OX_1 receptor are important for the induction of cellular apoptosis mediated by the orexin-B/OX_1 receptor interaction. As the OX_1 receptor is aberrantly expressed in colon cancer and its activation by exogenous orexins results in robust apoptosis and strong inhibition of tumour development in preclinical animal models (Voisin *et al*., 2011), the design of full agonist peptide or non-peptide molecules represents a major challenge in new therapeutic approaches for the treatment of digestive cancers. The knowledge of the structure–function relationship of orexin-B and its receptor towards their pro-apoptotic responses advanced by this study represents a key step in the development of such molecules.

Acknowledgements

This study was supported by INSERM U1149/The Inflammation Research Center (CRI), The Institut National du Cancer (INCA) (translational project N°2013-213) and the Ligue contre le Cancer (RS 12/75-64). The authors wish to thank Dr Martine Torres for the critical reading of the manuscript and editorial help.

Author contributions

P. N. carried out the alanine scanning of orexin-B experiments including binding tests, apoptosis and IP_3 measurement and participated to the construction of OX_1 receptor mutants and their characterization. P. C. performed OX_1 receptor mutants construction and their characterization; T. V. contributed to the study design and co-analysed results with A. C. N. J.

built the OX_1 receptor and OX_1 receptor–orexin-B models and performed MD simulations. A. C. supervised all experiments, developed the OX_1 receptor 3D model, and wrote the manuscript.

Conflict of interest

The authors disclose no conflict of interest.

References

Alexander SPH, Benson HE, Faccenda E, Pawson AJ, Sharman JL, Spedding M *et al.* (2013a). The Concise Guide to PHARMACOLOGY 2013/14: G protein-coupled receptors. Br J Pharmacol. 170: 1459–1581.

Alexander SPH, Benson HE, Faccenda E, Pawson AJ, Sharman JL, Spedding M *et al.* (2013b). The Concise Guide to PHARMACOLOGY 2013/14: enzymes. Br J Pharmacol. 170: 1797–1867.

Alexandre D, Hautot C, Mehio M, Jeandel L, Courel M, Voisin T *et al.* (2014). The orexin type 1 receptor is overexpressed in advanced prostate cancer with a neuroendocrine differentiation, and mediates apoptosis. Eur J Cancer. 50: 2126–33.

Arnold K, Bordoli L, Kopp J, Schwede T (2006). The SWISS-MODEL workspace: a web-based environment for protein structure homology modelling. Bioinformatics. 22: 195–201.

Arunlakshana O, Schild HO (1959). Some quantitative uses of drug antagonists. Br J Pharmacol Chemother. 14: 48–58.

Asahi S, Egashira S, Matsuda M, Iwaasa H, Kanatani A, Ohkubo M *et al.* (2003). Development of an orexin-2 receptor selective agonist, [Ala(11), D-Leu(15)]orexin-B. Bioorg Med Chem Lett. 13: 111–113.

Benkert P, Biasini M, Schwede T (2011). Toward the estimation of the absolute quality of individual protein structure models. Bioinformatics. 27: 343–50.

Biasini M, Bienert S, Waterhouse A, Arnold K, Studer G, Schmidt T *et al.* (2014). SWISS-MODEL: modelling protein tertiary and quaternary structure using evolutionary information. Nucleic Acids Res. 42 (Web Server issue): W252–8.

Ceraudo E, Hierso R, Tan YV, Murail S, Rouyer-Fessard C, Nicole P *et al.* (2008). Spatial proximity between the VPAC1 receptor and the amino terminus of agonist and antagonist peptides reveals distinct sites of interaction. FASEB J. 26: 2060–71.

Ceraudo E, Murail S, Tan YV, Lacapère JJ, Neumann JM, Couvineau A *et al.* (2012). The vasoactive intestinal peptide (VIP) alpha-helix up to C terminus interacts with the N-terminal ectodomain of the human VIP/pituitary adenylate cyclase-activating peptide 1 receptor: photoaffinity, molecular modeling, and dynamics. Mol Endocrinol. 22: 147–55.

Darker JG, Porter RA, Eggleston DS, Smart D, Brough SJ, Sabido-David C *et al.* (2001). Structure-activity analysis of truncated orexin-A analogues at the orexin-1 receptor. Bioorg Med Chem Lett. 11: 737–40.

De Graaf C, Foata N, Engkvist O, Rognan D (2008). Molecular modeling of the second extracellular loop of G-protein coupled receptors and its implication on structure-based virtual screening. Proteins 71: 599–620.

El Firar A, Voisin T, Rouyer-Fessard C, Ostuni MA, Couvineau A, Laburthe M (2009). Discovery of a functional immunoreceptor tyrosine-based switch motif in a 7-transmembrane-spanning receptor: role in the orexin receptor OX1R-driven apoptosis. FASEB J. 23: 4069–80.

Fanelli F, De Benedetti PG (2011). Update 1 of: computational modeling approaches to structure–function analysis of G protein-coupled receptors. Chem Rev. 111: PR438–535.

German NA, Decker AM, Gilmour BP, Thomas BF, Zhang Y (2013). Truncated orexin peptides: structure–activity relationship studies. ACS Med Chem Lett. 4: 1224–1227.

Gotter AL, Webber AL, Coleman PJ, Renger JJ, Winrow CJ (2012). International Union of Basic and Clinical Pharmacology. LXXXVI. Orexin receptor function, nomenclature and pharmacology. Pharmacol Rev 64: 389–420.

Heifetz A, Barker O, Morris GB, Law RJ, Slack M, Biggin PC (2013). Toward an understanding of agonist binding to human orexin-1 and orexin-2 receptors with G-protein-coupled receptor modeling and site-directed mutagenesis. Biochemistry. 52: 8246–60.

Jo S, Kim T, Iyer VG, Im W (2008). CHARMM-GUI: a web-based graphical user interface for CHARMM. J Comput Chem. 29: 1859–65.

Klauda JB, Venable RM, Freites JA, O'Connor JW, Tobias DJ, Mondragon-Ramirez C *et al.* (2010). Update of the CHARMM all-atom additive force field for lipids: validation on six lipid types. J Phys Chem B. 114: 7830–43.

Kruse AC, Ring AM, Manglik A, Hu J, Hu K, Eitel K *et al.* (2013). Activation and allosteric modulation of a muscarinic acetylcholine receptor. Nature. 504: 101–6.

Laburthe M, Voisin T (2012). The orexin receptor OX(1)R in colon cancer: a promising therapeutic target and a new paradigm in G protein-coupled receptor signaling through ITIMs. Br J Pharmacol. 165: 1678–87.

Laburthe M, Voisin T, El Firar A (2010). Orexins/hypocretins and orexin receptors in apoptosis: a mini-review. Acta Physiol (Oxf). 198: 393–402.

Lang M, Soll RM, Durrenberger F, Dautzenberg FM, Beck-Sickinger AG (2004). Structure-activity studies of orexin a and orexin B at the human orexin 1 and orexin 2 receptors led to orexin 2 receptor selective and orexin 1 receptor preferring ligands. J Med Chem. 47: 1153–1160.

Lappano R, Maggiolini M (2011). G protein-coupled receptors: novel targets for drug discovery in cancer. Nat Rev Drug Discov. 10: 47–60.

Lee JH, Bang E, Chae KJ, Kim JY, Lee DW, Lee W (1999). Solution structure of a new hypothalamic neuropeptide, human hypocretin-2/orexin-B. Eur J Biochem. 266: 831–9.

Le Guilloux V, Schmidtke P, Tuffery P (2009). Fpocket: an open source platform for ligand pocket detection. BMC Bioinformatics. 10: 168.

MacKerell AD, Bashford D, Bellott M, Dunbrack RL, Evanseck JD, Field MJ *et al.* (1998). All-atom empirical potential for molecular modeling and dynamics studies of proteins. J Phys Chem B. 102: 3586–616.

Mackerell AD Jr, Feig M, Brooks CL 3rd. (2004). Extending the treatment of backbone energetics in protein force fields: limitations of gas-phase quantum mechanics in reproducing protein conformational distributions in molecular dynamics simulations. J Comput Chem. 25: 1400–15.

Nicole P, Lins L, Rouyer-Fessard C, Drouot C, Fulcrand P, Thomas A *et al.* (2000). Identification of key residues for interaction of vasoactive intestinal peptide with human VPAC1 and VPAC2 receptors and development of a highly selective VPAC1 receptor agonist. Alanine scanning and molecular modeling of the peptide. J Biol Chem. 275: 24003–12.

Pawson AJ, Sharman JL, Benson HE, Faccenda E, Alexander SP, Buneman OP, Davenport AP, McGrath JC, Peters JA, Southan C, Spedding M, Yu W, Harmar AJ; NC-IUPHAR. (2014) The IUPHAR/BPS

Guide to PHARMACOLOGY: an expert-driven knowledgebase of drug targets and their ligands. Nucl. Acids Res. 42 (Database Issue): D1098-106.

Preininger AM, Meiler J, Hamm HE (2013). Conformational flexibility and structural dynamics in GPCR-mediated G protein activation: a perspective. J Mol Biol. 425: 2288–98.

Rasmussen SG, DeVree BT, Zou Y, Kruse AC, Chung KY, Kobilka TS *et al.* (2011a). Crystal structure of the β2 adrenergic receptor-Gs protein complex. Nature. 477: 549–55.

Rasmussen SG, Choi HJ, Fung JJ, Pardon E, Casarosa P, Chae PS *et al.* (2011b). Structure of a nanobody-stabilized active state of the β(2) adrenoceptor. Nature. 469: 175–80.

Rouet-Benzineb P, Rouyer-Fessard C, Jarry A, Avondo V, Pouzet C, Yanagisawa M *et al.* (2004). Orexins acting at native OX(1) receptor in colon cancer and neuroblastoma cells or at recombinant OX(1) receptor suppress cell growth by inducing apoptosis. J Biol Chem. 279: 45875–86.

Thompson MD, Xhaard H, Sakurai T, Rainero I, Kukkonen JP (2014). OX1 and OX2 orexin/hypocretin receptor pharmacogenetics. Front Neurosci. 57: 1–12.

Venkatakrishnan AJ, Deupi X, Lebon G, Tate CG, Schertler GF, Babu MM (2013). Molecular signatures of G-protein-coupled receptors. Nature. 494: 185–94.

Voisin T, El Firar A, Fasseu M, Rouyer-Fessard C, Descatoire V, Walker F *et al.* (2011). Aberrant expression of OX1 receptors for orexins in colon cancers and liver metastases: an openable gate to apoptosis. Cancer Res. 71: 3341–51.

Voisin T, El Firar A, Rouyer-Fessard C, Gratio V, Laburthe M (2008). A hallmark of immunoreceptor, the tyrosine-based inhibitory motif ITIM, is present in the G protein-coupled receptor OX1R for orexins and drives apoptosis: a novel mechanism. FASEB J. 22: 1993–2002.

Voisin T, Firar AE, Avondo V, Laburthe M (2006). Orexin-induced apoptosis: the key role of the seven-transmembrane domain orexin type 2 receptor. Endocrinology. 147: 4977–84.

Wu EL, Cheng X, Jo S, Rui H, Song KC, Dávila-Contreras EM *et al.* (2014). CHARMM-GUI membrane builder toward realistic biological membrane simulations. J Comput Chem. 35: 1997–2004.

Xu TR, Yang Y, Ward R, Gao L, Liu Y (2013). Orexin receptors: multi-functional therapeutic targets for sleeping disorders, eating disorders, drug addiction, cancers and other physiological disorders. Cell Signal. 25: 2413–23.

Yin J, Mobarec JC, Kolb P, Rosenbaum DM (2015). Crystal structure of the human OX2 orexin receptor bound to the insomnia drug suvorexant. Nature. 519: 247–50.

Supporting Information

Additional Supporting Information may be found in the online version of this article at the publisher's web-site:

http://dx.doi.org/10.1111/bph.13287

Figure S1A and S1B Specific ^{125}I-OxA binding to CHO-S-OX1R cells in the presence of increasing concentrations of unlabeled OxB and OxB analogs as indicated in figure (*left*) and determination of the stimulation of IP3 production (*middle*) or the inhibition of cellular growth induced (*right*) by increasing concentrations of OxB and OxB analogs in CHO-S-OX1R cells. CHO-S-OX1R cells were incubated with the indicated concentrations of OxB (◯) and OxB analogs (●). *Left*, results are expressed as the percentage of radioactivity specifically bound in the absence of added unlabeled peptide; Middle, results are expressed as the percentage of maximal IP3 production; *Right*, results are expressed as the percentage of total viable cells. Each point is the mean of three separate experiments. For the sake of clarity, standard errors are not indicated. They were always below 15% of mean values.

Figure S2 Antagonism S18A/N20A and S18A/T27A was analysed by a Schild plot in which antagonism was expressed by the dose ratios of OxB needed to produce half-maximal responses in the absence and the presence of different concentrations of S18A/N20A (*left panel*) or S18A/T27A (*right panel*). Dose ratios were estimated graphically in three separate experiments as shown in figure 3C and 3D. The regression line was calculated by the method of the least square.

Figure S3 Snapshot representation of the system composed of the OXR1-OxB complex embedded in a POPC bilayer and water and ions. OXR1 and OxB are represented as a yellow and a red ribbon, respectively. The POPC lipids are in blue sticks without the hydrogen atoms for sake of clarity. Potassium and chloride ions are represented as Van der Waals spheres colored in blue and orange, respectively. Water molecules are in red.

Figure S4 Molecular dynamic simulation of the complex OX1R/OxB20-28. Conformational drift from initial structure during the simulation (100 ns) measured as backbone rmsd for the complex OX1R/OxB20-28. Values for TM1 to TM7 as indicated in the figure, were represented.

Figure S5 Molecular dynamic simulation of the complex OX1R/OxB20-28. Conformational drift from initial structure during the simulation (100 ns) measured as backbone rmsd for the complex OX1R/OxB20-28. Values for Interface helix, β1-β2 and OxB20-28 as indicated in the figure, were represented.

Figure S6 Stability of the secondary structure of OxB20-28 as a function of time during the MD trajectory. The X axis represents the MD trajectory time (in ns), while the residues are shown on the Y-axis. Color indicates secondary structure elements: alpha helical structure is in pink, 3-10 helical structure in blue, turn in green and random coil in white. The graph was generated using VMD timeline tool. (Humphrey, W., Dalke, A. and Schulten, K., "VMD - Visual Molecular Dynamics", J. Molec. Graphics, 1996, vol. 14, pp. 33–38.).

Figure S7 Putative 3D-model of human OX1R (turquoise) docked to sequence of OxB (red). The full sequence (1–28) of OxB was structurally aligned to 3D model of the complex OX1R/OxB6-28 using Chimera software (http://www.cgl.ucsf.edu/chimera/)